Computational Materials Science 191 (2021) 110326

Contents lists available at ScienceDirect

Computational Materials Science

journal homepage: www.elsevier.com/locate/commatsci

A theoretical calculation of stacking fault energy of Ni alloys: The effects of temperature and composition

Mohammad S. Dodaran [a,b], Shengmin Guo [c], Michael M. Khonsari [c], Nima Shamsaei [a,b], Shuai Shao [a,b,*]

[a] Department of Mechanical Engineering, Auburn University, Auburn, AL 36849, USA
[b] National Center for Additive Manufacturing Excellence (NCAME), Auburn University, Auburn, AL 36849, USA
[c] Department of Mechanical and Industrial Engineering, Louisiana State University, Baton Rouge, LA 70803, USA

ARTICLE INFO

Keywords:
Ni superalloys
Stacking fault energy
Cluster expansion
Density functional theory
One dimensional axial Ising model

ABSTRACT

Combining cluster expansion (CE) method with one dimensional axial Ising model, this work investigated the effects of alloying elements and configurational variations due to temperature on the stacking fault energy (SFE) of FCC Ni binary alloys. Ensembles of large numbers of atomistic structures, each with more than ~400 atoms, were generated to consider sufficient long-range chemical disorder and temperature effects due to configurational entropy. A Monte Carlo Metropolis algorithm was used to generate these structures, whose energies were then evaluated based on the effective cluster interactions obtained from CE. As a baseline, this work had shown the SFE of pure Ni and Al to be 127 mJ/m^2 and 137 mJ/m^2, respectively, which agreed with the experimental values of 125 mJ/m^2 and 150 mJ/m^2 reported in the literature. Additions of Al, Ti, Cr and Co to pure Ni were found to decrease the SFE to different extents. Although temperature does not strongly influence the SFE of the FCC Ni-Al and Ni-Cr binary alloys, it can lead to significant changes to the SFE of the FCC Ni-Ti and Ni-Co alloys. While effects of temperature and composition on SFE observed in this work were calculated from binary Ni alloys, the general trends are nonetheless expected to be valid in the γ phase of multicomponent Ni superalloys.

1. Introduction

Ni superalloys, owing to their exceptional thermal–mechanical properties at elevated temperatures and in corrosive environments, find applications under extreme conditions, such as ones encountered in gas turbines and power plants [1–4]. The alloys' superior high-temperature strength is primarily ascribed to a solid solution strengthened FCC matrix (γ) that can also be strengthened by γ' and/or γ" intermetallic precipitates. The γ' precipitates have an $L1_2$ ordered lattice structure and are typically coherent with the γ matrix. The existence of Nb and Fe are believed to result in precipitation of another ordered phase, with $D0_{22}$ lattice structure, known as γ" which is typically disk-shaped [5,6]. The γ" is semicoherent with the γ matrix and is at a significantly larger lattice mismatch— ~3.0% or ~0.5% depending on the crystallographic orientation [7].

Other phases, such as topologically close packed phases and various forms of carbides, are observed mostly at grain boundaries. These phases do not significantly contribute to the strength of the material, but can prevent grain boundary sliding and improve the creep properties of the alloy [8]. While the precipitates impede the gliding motion of dislocations and are primarily responsible for the strengthening in Ni superalloys, the more compliant γ matrix accommodates plasticity better and is more susceptible to plasticity induced damage [9]. As is well known, a strong influencing factor for plasticity occurring in the γ phase is the stacking fault energy (SFE) [10,11].

In FCC crystals, a perfect dislocation dissociates into Shockley partials, bounding a stacking fault, to reduce the dislocation line energy. The width of the stacking fault is determined by the energy balance between the repelling partial dislocations and the fault's excess energy. The equilibrium distance between the Shockley partials is therefore given as:

$$d_{eq} = \frac{Gb^2}{\gamma_{SFE}} f \tag{1}$$

where d_{eq} is the equilibrium distance of the Shockley partials, G is the shear modulus, b is the magnitude of the Burgers vectors of the partials,

* Corresponding author at: Department of Mechanical Engineering, Auburn University, Auburn, AL 36849, USA.
E-mail address: sshao@auburn.edu (S. Shao).

https://doi.org/10.1016/j.commatsci.2021.110326
Received 30 August 2020; Received in revised form 15 January 2021; Accepted 16 January 2021
Available online 8 February 2021

γ_{SFE} is the SFE, and f is a geometrical factor that depends on the dislocations' character [12,13]. Using this relation, transmission electron microscopy is typically used to measure the SFE by measuring the separation distance between a partial dislocation pair [14,15].

Applied stress, temperature, and SFE dictate the activation of different mechanisms occurring during slip, such as cross slip and climb [16–18]. Cross slip can happen via the Friedel-Escaig (FE) mechanism [19–21], in which an extended core will constrict locally and dissociate again onto another slip plane [22]. Accordingly, the reduction in the SFE will increase the energy barrier for the cross slip. Similarly, dissociation of perfect dislocations into Shockley partials also results in the reduction of climb-rate as constriction is required prior to the climb of a dislocation. Indeed, Argon et al., using a hard-sphere model, demonstrated that the climb velocity of an extended jog is reduced as the SFE is reduced [23]. Experimental results also indicate that higher SFEs lead to higher creep rates [24–26] in dislocation creep regime, indicating the positive influence of SFE on the dislocation climb rate.

SFE is strongly influenced by local chemistry [27]. The complex chemical composition of the Ni superalloys makes it difficult to account for the effect of all atomic species in numerical calculations. For instance, both molecular dynamics (MD) simulations and density functional theory (DFT) had been used to evaluate SFE using the supercell approach or the axial Ising model (AIM) [28–31]. The supercell approach calculates the SFE by comparing the total energies of perfect and faulted structures. However, the main drawback of MD had been the lack of accurate interatomic potentials that can represent multiple atomic species. On the other hand, DFT calculations, although capable of modeling the interactions among multiple atomic species, are computationally limited. In addition, the interaction between different chemical species with the stacking fault tends to strongly influence the results of the calculations [32]. Direct DFT calculations with the supercell approach had been performed with only a few tens of atoms [29]. As a result, increasing the number of the random configurations (each containing 24 atoms) from 4 to 25 have led to a change in SFE by 20–30 mJ/m^2.

In contrast to the supercell approach, the AIM is regarded as a "non-local" method and does not explicitly consider the location of a specific stacking fault. When combined with DFT, it can produce more reliable, "averaged" SFE values [29,33,34]. However, due to DFT's inherent limitation in the computational length scale, the effect of chemical disordering in the alloys still cannot be properly accounted for. To this end, statistical mechanical models, such as the cluster expansion (CE) method, may help overcome the length scale barriers of DFT. Indeed, the DFT + CE framework had been successfully applied to investigate the effects of temperature and composition on the antiphase boundary energy in Ni superalloys [35,36].

In this work, a combination of DFT, cluster expansion (CE), and AIM have been used to determine the SFE of FCC $Ni_xM_{(1-x)}$ alloys (M = Al, Ti, Cr, and Co) in a temperature range that is likely to be encountered by Ni superalloys during service. The results shed light into the general effects of solutes and configurational variations due to temperature on the SFE of Ni superalloys. With the effective cluster interactions determined by CE, the chemical disordering effect was captured by calculating the energies of 1000+ randomized atomistic configurations per composition—each of such configurations contained more than ~400 atoms. For each composition, three different crystal structures, namely FCC, HCP, and double hexagonal close-packed (DHCP), were considered to formally establish the second nearest-neighbor AIM. In what follows, the temperature effects on the SFE originating from configurational entropy is referred to as the "configurational temperature effect". This article first explains the utilized methodology and describes the investigated material system in Section 2. Section 3 presents the main findings of this study and discusses the effect of solutes, configurational temperature effect, and their synergy on the SFE of Ni binary alloys. Finally, the conclusions are drawn in Section 4.

2. Methodology and computational details

Using AIM combined with CE and Monte Carlo (MC) sampling, the SFE of binary FCC $Ni_xM_{(1-x)}$ alloys is calculated at a range of temperatures. Since the service temperature of most Ni superalloys are generally below 1100 K, it has been selected as the maximum temperature in the current study. Due to their high mechanical strengths and good corrosion resistance, many Ni superalloys are also used in the room temperature. Therefore, the temperatures considered in this study are 300 K, 700 K, and 1100 K. The approach, as summarized in the Graphical Abstract, include: (1) parameterization of the interaction between dissimilar atoms in an alloying environment using CE and DFT calculations in FCC, HCP, and DHCP lattices; (2) calculation of average per atom energies of the randomized atomistic configurations under three parent lattice structures at each composition; and (3) calculation of SFE at each composition using AIM. This section provides details regarding each part of the procedure, including the AIM, CE, and DFT.

2.1. Axial Ising model (AIM)

AIM approach is adopted in this work to overcome the shortcomings of the supercell approach with DFT calculations, i.e. the undesired interactions between a stacking fault and its periodic images. Within the supercell approach, if the effects of such interactions are to be minimized, the number of atoms within the cell would have to be increased, and—if the random nature of the solid solution is to be captured—it will likely exceed the capability of the DFT method (100–200 atoms).

In these cases, energy parametrization seems to be a viable alternative. Indeed, the AIM, which was adapted from the generalized Ising model, has been utilized to parametrize energies of atomic structures composed of periodic stacking of atomic layers [33,34,37,38]. In this method, a spin parameter, S_i, taking the values ± 1, will be assigned to each layer based on the stacking of the next layer. For instance, in an FCC structure, if layer $i+1$ conforms to the perfect stacking sequence, S_i will be $+1$. Otherwise, S_i will be assigned -1. As an example, the spin parameters assigned to a stacking such as, …ABCBC…, would be shown in up/down spin notation as ↑↑↓↑↑, and the corresponding spin parameters would be 1, 1, −1, 1, 1. Having defined the spin parameters, the energy of an atomic stack can be calculated as:

$$E = J_0 - J_1 \sum_i S_i S_{i+1} - J_2 \sum_i S_i S_{i+2} - J_3 \sum_i S_i S_{i+3} - \cdots \quad (2)$$

where J_i are the interaction coefficients having the units of energy, which can be obtained by equating Eq. (2) to the calculated energy of atomic stacks using numerical methods such as DFT and solving the corresponding linear systems of equations. The number of solvable interaction coefficients, J_i, depends on the available number of atomic stacks with known energies. The values of the interaction coefficients measure how strongly a particular atomic layer interacts with its neighbors, i.e. J_0 indicates self-interaction, J_1 indicates nearest-neighbor interaction, J_2 indicates second nearest-neighbor interaction, etc.

Theoretical works have shown that the second-order expression considering the interaction of next-nearest neighbors within AIM model is accurate enough to parametrize the energy of atomic stacks [39,40]. This work, therefore, only considers J_i where $i \leq 2$. The energy per layer of the stack in each of the parent lattices is (here the lower case e is used to denote the per layer energy):

$$\begin{aligned} e_{ABC} &= J_0 - J_1 - J_2 - O(J_3) + \\ e_{AB} &= J_0 + J_1 - J_2 + O(J_3) + \cdots \\ e_{ABCB} &= J_0 + J_2 + O(J_3) \end{aligned} \quad (3)$$

Solving Eq. (3), one can obtain the interaction coefficients. Isolating a single fault within the structure by increasing the number of layers to infinity, the SFE can be calculated by subtracting the energy

polynomials as:

$$E_{ISF} - E_{FCC} = \gamma_{ISF} A_{ISF} = 4J_1 + 4J_2 \quad (4)$$

where A_{ISF} is the area of the stacking fault, E_{ISF} and E_{FCC} are the total energies of structures containing only one intrinsic stacking fault (ISF) and no stacking fault, respectively. For any compositions listed in Table 1, three different stacking sequences, namely ABC (FCC), AB (HCP), and ABCB (DHCP) (shown in Fig. 1), have been considered to calculate the interaction coefficients appearing in Eq. (2). Substituting Eq. (3) into Eq. (4), the intrinsic SFE can also be calculated by directly substituting the per layer, energy of these three stacking sequences, i.e.

$$\gamma_{ISF} A_{ISF} = e_{AB} + 2e_{ABCB} - 3e_{ABC} \quad (5)$$

Each term appearing in Eq. (5) are the mean values obtained by averaging the per atom (normalized to the case of one atom per layer) energies of over 1000 variations in the atomic configurations, constructed by MC sampling scheme and evaluated by CE method.

2.2. Cluster expansion (CE)

Energies of the atomic stacks used to solve for the interaction coefficients in Eq. (2) are obtained using the CE method [41] via the ATAT toolkit developed by van de Walle et al. [42]. For each composition, ~1000 randomized configurations/clusters of atoms representing alloying elements in a disordered solid solution are considered and their mean energy value obtained. In CE formalism, any configuration dependent function, including energy, can be expressed using orthogonal cluster functions ($\varphi_{\alpha s}$) and the so-called effective cluster interactions ($K_{\alpha s}$) i.e.

$$E(\sigma) = \sum_{\alpha} \sum_{s} K_{\alpha s} \varphi_{\alpha s}(\sigma), \quad (6)$$

where α is the designation used for each cluster of atoms and s is the order of the orthogonal polynomial used to describe the cluster functions [41,44,45]. The effective cluster interactions ($K_{\alpha s}$) can be fitted to the energies of small atomic clusters. No more than ~10 atoms [43], obtained from DFT calculations (such as the ones shown in the top and middle rows of Fig. 2). The accuracy of the CE, is measured by cross-validation (CV) score:

$$CV = \sqrt{\frac{1}{n} \sum_{i=1}^{n} \left(E_i - \widehat{E}_i \right)^2} \quad (7)$$

where n is the total number of structures used to obtain the cluster interaction coefficients, E_i is the energy of the cluster i using DFT calculation, and $\widehat{E}_i$ is the energy obtained by CE using all the structures except for cluster i to calculate the interaction coefficients.

As SFE is sensitive to the local chemistry, the chemical disorder effect on the SFE can only be considered when enough structures are generated and their mean energy value obtained. For this purpose, starting from an initial structure, MC sampling is performed with the Metropolis algorithm to swap atoms within the lattice structure. Note that the MC "randomization" is needed as structures with lower energies are more probable to occur [46]. Starting with the initial atomistic configuration as the reference structure, if the new structure generated has lower energy, i.e. $\Delta E = E_1 - E_0 < 0$, the new cluster will be accepted as a new reference configuration. Otherwise, a temperature-dependent probability, $\exp(-\Delta E/k_b T)$, will be assigned for the acceptance of the new configuration. Here, k_b is the Boltzmann constant, and T is the temperature in the units of Kelvin. At any given composition and temperature, configurational variations in the atomic structures generated by the aforementioned procedure may induce fluctuations in the SFE, which can be estimated based on the standard deviation (SD) of the energies of these structures under each parent lattice. According to Eq. (5), an upper bound estimation of the SD of γ_{ISF} can be calculated as:

$$SD(\gamma_{ISF}) = 1/A_{ISF} [SD(e_{AB}) + 2 \times SD(e_{ABCB}) + 3 \times SD(e_{ABC})] \quad (8)$$

where $SD(\gamma_{ISF})$ accounts for the natural fluctuation in the SFE due to configurational entropy, $SD(e_{AB})$, $SD(e_{ABC})$, and $SD(e_{ABCB})$ are the SDs of the per-atom energies of the HCP, FCC, and DHCP structures generated by MC, respectively. As shown, the SDs of the per-atom energies of all lattice structures superimpose constructively in the calculation of SD (γ_{ISF}).

Since Eq. (5) is extremely sensitive to error, correction factors based on the difference in the energies obtained from DFT and CE performed on pure systems are considered for each element type. Note that the correction factors for a specific material vary by the change of the parent lattice.

The advantages of using CE method over conventional direct DFT to calculate the energy of an atomic structure are twofold. First, many more different configurations can be calculated using CE, which incorporates the effect of chemical disorder. Second, since CE can calculate much larger atomic clusters, much more dilute solid solutions can be accessed (compare 1 solute atom in a 10-atom cluster vs. 1 solute atom in a 400-atom cluster).

2.3. Correlating CE of different parent lattices

Within CE, the calculated per-atom energy of material with parent lattice-type β is presented as

$$E_{\beta}^{CE} = \sum_{i=1}^{n} x_i E_i^{pure} + \Delta E_{inter} \quad (9)$$

where the sum is taken over all atom types that exist in the configuration, x_i is the concentration of atom type i, E_i^{pure} is the per-atom energy of atom i in the pure limit, and ΔE_{inter} is the interaction energy of dissimilar atoms within the configuration. Although the CE produces energies of atomistic configurations with relatively good accuracy (CV is below 0.020 eV/atom for all cases), when performed on different parent lattices, it may give rise to small systematic errors that may accumulate due to the form of Eq. (5). As such, the energy terms used in Eq. (5) are obtained from Eq. (9) and adjusted based on a correction factor.

The correction factors are obtained in the limit of pure materials using the per atoms energies acquired from DFT calculations ($E_i^{DFT-pure}$) as a reference, i.e.

$$C_{Cor.} = \frac{E_i^{DFT-pure}}{E_i^{pure}}. \quad (10)$$

Thus, the final form of the calculated energy for parent lattice-type β that will be substituted in Eq. (5) is calculated as:

$$E_{\beta} = \sum_{i=1}^{n} C_{cor.} E_i^{pure} x_i + \Delta E_{inter} \quad (11)$$

Note that in Eq. (11), ΔE_{inter} is a mean value evaluated based on 1000 or more atomic configurations. In addition, ΔE_{inter} is solely due to the configurational variations induced by finite temperatures – vibrational entropic effects [47] are not included.

Table 1
Compositional ranges of the binary $Ni_xM_{(1-x)}$ alloys considered in the present work and the solubility of various elements in Ni.

Alloying element	Solute Concentration at.%					Solubility @700 K at.%	Solubility @1100 K at.%
Al	5	10	15	20	25	11	15
Ti	5	10	15	–	–	~7	12
Cr	9	18	27	36	45	36	47
Co	15	30	45	60	75	100	100

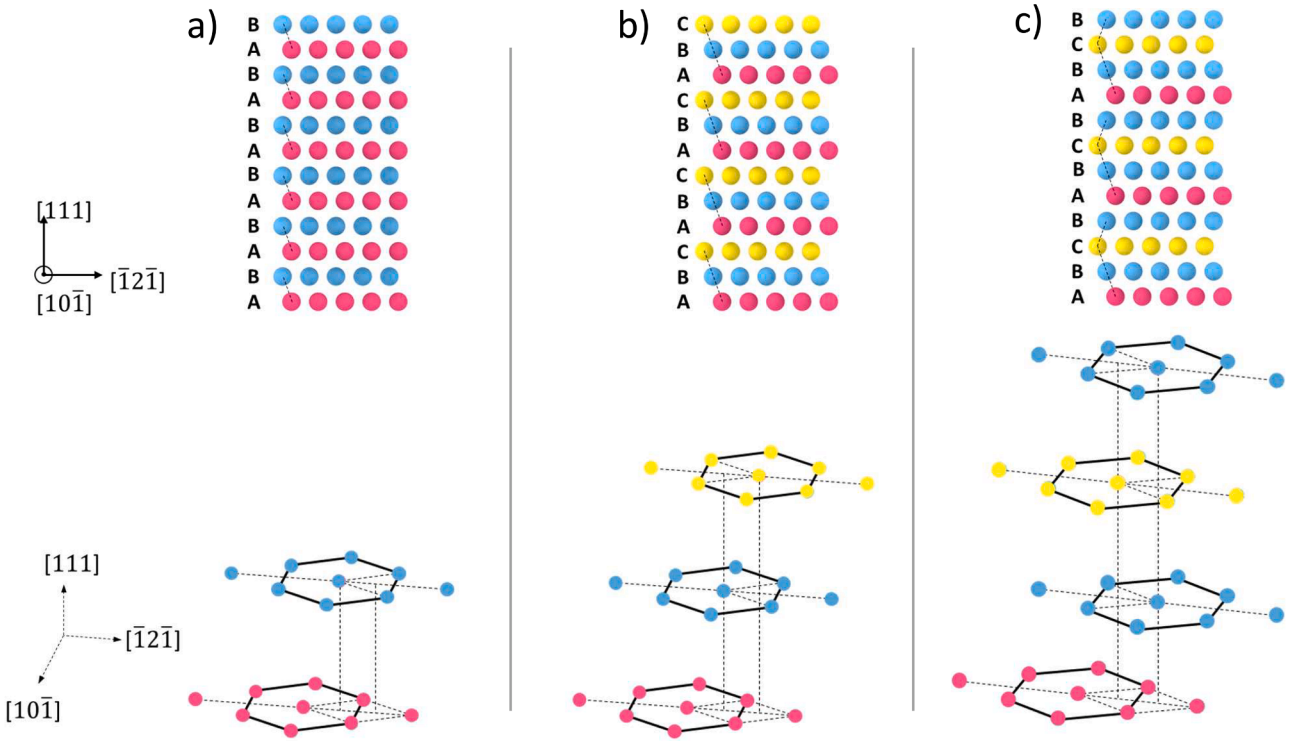

Fig. 1. Different stacking along ⟨1 1 1⟩ direction, used in Axial Ising model: a) HCP, b) FCC, and c) DHCP.

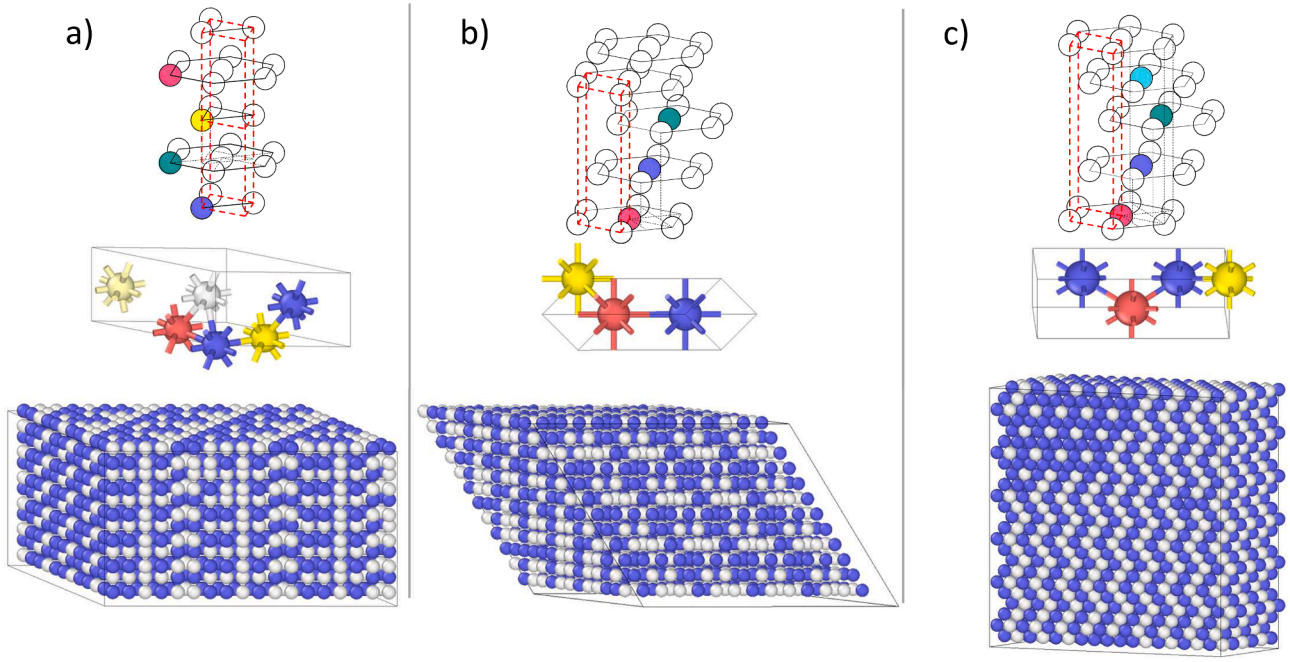

Fig. 2. Top and middle row: schematic representation vs actual geometries of supercells relaxed by DFT calculations for different parent lattices: a) HCP, b) FCC, and c) DHCP. Bottom row: actual supercells whose energies are calculated by cluster expansion (CE).

2.4. Density functional theory

To obtain the energies of the atomic clusters (such as ones shown in the bottom row of Fig. 2) for CE, first-principle calculations based on DFT as implemented in Quantum Espresso package has been performed. These small atomic clusters are periodic and typically contain no more than ~10 atoms (such as the schematic representations and the actual geometries shown in the top and middle rows of Fig. 2) [43]. The pseudopotentials have been obtained from the standard solid state pseudopotential (SSSP) repository [48]. The combined effect of nuclei and core electrons with the valence electrons is incorporated using the projector augmented wave (PAW) method for Al, while ultrasoft pseudopotentials are used for the rest of elements, i.e Ni, Ti, Cr, and Co. The Perdew-Burke-Ernzerhof parametrized form of the generalized gradient approximation for the true exchange and correlation functional is used in self-consistent calculations [49]. A plain wave basis with 35 Ry (476

eV) energy cutoff is used to expand the wave functions. For the integration over the Brillion zone, the Monkhorst-Pack scheme has been used for k-point sampling with the k-point density of 0.02–0.03 Å in the reciprocal space. Necessary spin polarization is used whenever the clusters contain magnetic elements such as Ni, Cr, and Co. The energy convergence criterion for self-consistent energy calculation is 10^{-7} Ry. To verify the accuracy of the pseudopotentials used, the lattice parameters and the elastic constants of the pure elements were calculated and compared to data available in literature. The results of such comparison were provided in the authors' earlier work [36]. For all three parent lattices, i.e. FCC, HCP, and DHCP, the volumetric relaxation is performed while keeping the ions fixed and maintaining the lattice symmetry. This technique has proven to yield results in good agreement with the experiments, since chemical disorder was shown to have more influence on the SFE [29,36].

3. Results and discussion

3.1. SFE of pure FCC crystals from DFT

To establish a baseline and confidence in the methodology adopted in this study, the SFEs of pure Ni and Al crystals are first calculated using DFT combined with AIM and compared with the literature. Since there is no chemical disorder effect in the case of pure crystals, direct DFT calculations are used to obtain energies of the three parent lattices, including FCC, HCP, and DHCP. Computational details regarding DFT calculations are similar to what has been mentioned in Section 2.4. Ground state lattice structures are acquired by fitting the Murnaghan equation of state to a series of structures, with varying cell parameters [50]. The equilibrium lattice parameters of the FCC structures are also obtained from this procedure and are used to calculate the per atom area on the {1 1 1} lattice planes. Resulting SFE of pure Ni and Al are presented in Table 2 along with the data available in the literature. The calculated SFE value in this study for Ni is 127.37 mJ/m^2, and for Al this value is 137.44 mJ/m^2, respectively, which resides well within the reported ranges by both experimental and numerical studies. For instance, Carter et al. have measured the equilibrium distance of a dissociated edge dislocation using weak beam transmission electron microscopy (TEM) and obtained the SFE of Ni to be within the range 120–130 mJ/m^2 [14]. Experimentally measured intrinsic SFE of Al is reported to be 135 ± 20 mJ/m^2 [51].

Next, to calculate the correction factors introduced in Eq. (11), the per-atom energies of prototypical FCC, HCP, and DHCP lattices for other elements considered in this study, i.e. Ti, Cr, and Co, are calculated using DFT as well. Accordingly, the determined correction factors ($C_{Cor.}$) are included in Table 3.

Table 2
SFE of pure Ni and Al.

Al	$\gamma_{SF}(mJ/m^2)$	Ref	Ni	$\gamma_{SF}(mJ/m^2)$	Ref
This study	137.44		This study	127.37	
Exp.	280±50	[67]	Exp.	125	[13]
	135±20	[51]		214	[68]
	166	[69]		120–130	[14]
	150±40	[70]		128	[69]
Sim.	144 (MD)	[31]	Sim.	134 (MD)	[71]
	158 (DFT)	[72]		137 (MD)	[73]
	124 (MD)	[74]		125 (MD)	[75]
	124 (DFT)	[76]		110 (DFT)	[77]
	130 (DFT)	[78]		133 (DFT)	[79]
	146 (DFT)	[75]		127 (DFT)	[79]
	164 (DFT)	[80]		129 (MD)	[81]
	203 ± 77 (DFT)	[82]		262 (DFT)	[83]

3.2. Multicomponent CE parameterization

Compositional range for each binary alloy (1-x for $Ni_xM_{(1-x)}$, where M = Al, Ti, Cr, or Co) is decided such that only the disordered FCC solid solution forms throughout. Therefore, the range of compositions selected for CE of all parent lattices should cover the compositions investigated here. Based on the binary phase diagram of Ni-Al [52] starting from 300 K up to 1100 K, the solubility of Al linearly increases from 7.5 at.% to ~15 at.%. The excess Al dissolved into the Ni matrix above the mentioned threshold will form the ordered $L1_2$ γ' phase. Since the lattice structure of the γ' phase exactly matches that of the FCC parent lattice, the resulting energy values obtained from CE are still valid as a measure of the complex stacking fault energy [53]. On the other hand, Ni matrix can hold a maximum amount of ~15 at.% of Ti at 1300 K. Lower temperatures at this composition or excess Ti solute addition to the system will result in precipitation of the Ni_3Ti compound [54]. The equilibrium lattice structure of this phase is hexagonal $D0_{24}$ [55]. Consequently, the CE performed using FCC parent lattice is no longer applicable to this phase. Therefore, the maximum concentration of Ti is limited to ~15 at.%.

For Cr and Co, based on the phase diagram, in order to have a single-phase solid solution compatible with the FCC lattice structure, a maximum of 45 at.% and 75 at.% percent solute can be added, respectively [56–58]. Note that above the Co's transition temperature (from HCP to FCC) Ni and Co are infinitely soluble. However, to avoid the formation of HCP phases at room temperature, the solute concentration is limited to 75 at.%. As listed in Table 1 for all the solute elements, multiple equally spaced compositional intervals are designed to capture the solute effect on the SFE. For all compositions listed above, the configuration-dependent energies are obtained using the multicomponent CE with correction factors applied (see Eq. (11)).

Details regarding the multicomponent CE performed in this study are included in Table 4. In all three cases, a minimum of 25 at.% Ni is defined as the constraint by which the clusters are generated, and effective cluster interactions are obtained. As shown, all three CEs are resulting in energy values that are close to the exact energy values, evidenced by the cross-validation score of 0.0114, 0.0163 and 0.0189 meV/atom are obtained for the HCP, FCC and DHCP parent lattices, respectively. Using MC metropolis algorithm, a minimum of 1000 structures are generated and calculated for each parent lattice types and at each composition, reaching a convergence of the mean energy. In all cases, convergence is ensured within a threshold of 1 meV/atom. Typical convergence behavior of 15 at.% Al within the Ni matrix is shown in Fig. 3.

3.3. SFE of binary alloys at room temperature

The variation of SFE due to solute changes in binary alloys are measured by $\Delta\gamma_{ISF}$ – a relative SFE with respect to that of the pure Ni (127 mJ/m^2, see Table 2). The effect of solute concentration on the SFE of binary Ni-Al alloy at room temperature has been presented in Fig. 4(a) and compared to the values reported in the literature. As reported in the literature, with the increase of Al concentration up to ~10 at.%, the SFE significantly drops—as low as 60 mJ/m^2 (50% of the reference value) [59]. The energy drop calculated in this study is almost linear with the increase in Al concentration and agrees well with the reported experimental results. Note that the experimentally measured value of SFE for pure Ni in Fig. 4(a) is obtained from Hirth and Lothe and the results for alloyed metal by Al addition are taken from the study of Beeston et al. [13,60]. A similar descending trend was also reported by Nie et al. using MD, although the present work was able to capture the trend shown in the experiment more accurately [31]. Al concentrations beyond 15% lead to a drastic increase in SFE. This trend, although not reported in the literature, does seem intuitive as the Al concentration of 25% corresponds to the formation of Ni_3Al compound, which has a very high complex stacking fault energy of ~230 mJ/m^2 [53].

Table 3
Per atom energies obtained from DFT, predicted by CE, and correction factors obtained for different lattice structures to be used in the AIM.

	FCC			HCP			DHCP		
	DFT (eV/atom)	CE (eV/atom)	$C_{Cor.}$	DFT (eV/atom)	CE (eV/atom)	$C_{Cor.}$	DFT (eV/atom)	CE (eV/atom)	$C_{Cor.}$
Ni	−4670.232	−4670.254	0.9999953	−4670.217	−4670.223	0.9999986	−4670.222	−4670.261	0.9999916
Al	−537.4697	−537.2719	1.0003681	−537.433	−537.2068	1.0004217	−537.457	−537.3557	1.0001895
Ti	−1622.432	−1622.437	1.0000527	−1622.461	−1622.393	1.000011	−1622.441	−1622.328	1.0001154
Cr	−2387.312	−2387.324	1.0000105	−2387.264	−2387.216	0.9999895	−2387.299	−2387.408	1.0000547
Co	−4061.093	−4061.075	1.0000042	−4061.097	−4061.041	1.0000137	−4061.094	−4061.166	0.9999823

Table 4
Number of relaxed structures and cross validation scores for CE performed for the current study.

Structure	Number of clusters relaxed by DFT	Cross validation score (eV/atom)
HCP	1689	0.0114866
FCC	1669	0.0163439
DHCP	1725	0.0189006

On the other hand, this study indicated that the increase in Co content also decreases the SFE of the binary Ni-Co alloy at room temperature. Delehouzee et al. have experimentally measured the stacking fault density of multiple binary solid solutions and reported that the stacking fault density measured from alloy filings using X-ray diffraction analysis is inversely related to the SFE [61]. Using this relation, one can estimate the SFE of a $Ni_xM_{(1-x)}$ alloy based on its stacking fault density relative to the SFE and the stacking fault density of pure Ni. This procedure has shown a pronounced drop in SFE of binary Ni-Co alloys (red dashed line with hollow circles in Fig. 4(b)), which is in a good agreement with the present study. The experimental measurement from Koster et al. [62] by weak beam TEM is also in qualitative agreement with this study, although they reported a more significant rate of decline of SFE at the Co concentration of 55%~70%. As shown in Fig. 4(b), the discrepancy among the experimental data in the literature appears to have increased as the solute concentration decreases. The discrepancy is ~20 mJ/m^2 among these results at ~55 at.% Co concentration.

The comparison of results from multiple numerical studies on the effect of solute concentration on the SFE of Ni-Co binary alloys are also plotted in Fig. 4(b) [29,31,63]. Chandran et al. utilized a similar AIM based approach to capture the effect of alloying elements on the SFE of binary alloys, although they used direct DFT calculations within the framework of AIM. The computational cost of direct DFT calculations limits the total number of atomistic configurations that can be considered to account for the chemical disorder. In their study, an ensemble containing 30 different configurations was used at each composition. Data produced by Chandran et al. (green solid triangles in Fig. 4(b)) qualitatively agrees with this study and the experimental results, although relatively large scatter exists. The results from the MD calculations by Nie et al. [31] however, appear to overestimate the SFE compared to the experimental results—at 70 at.% Co concentration, the difference in SFE is ~20 mJ/m^2.

The effects Ti and Cr solution on room temperature SFE of the Ni-Ti and Ni-Cr binary alloys are presented in Fig. 4(c) and (d) and were compared to the limited data in the literature. The present study suggests that both Ti and Cr reduces the SFE, which is in general agreement

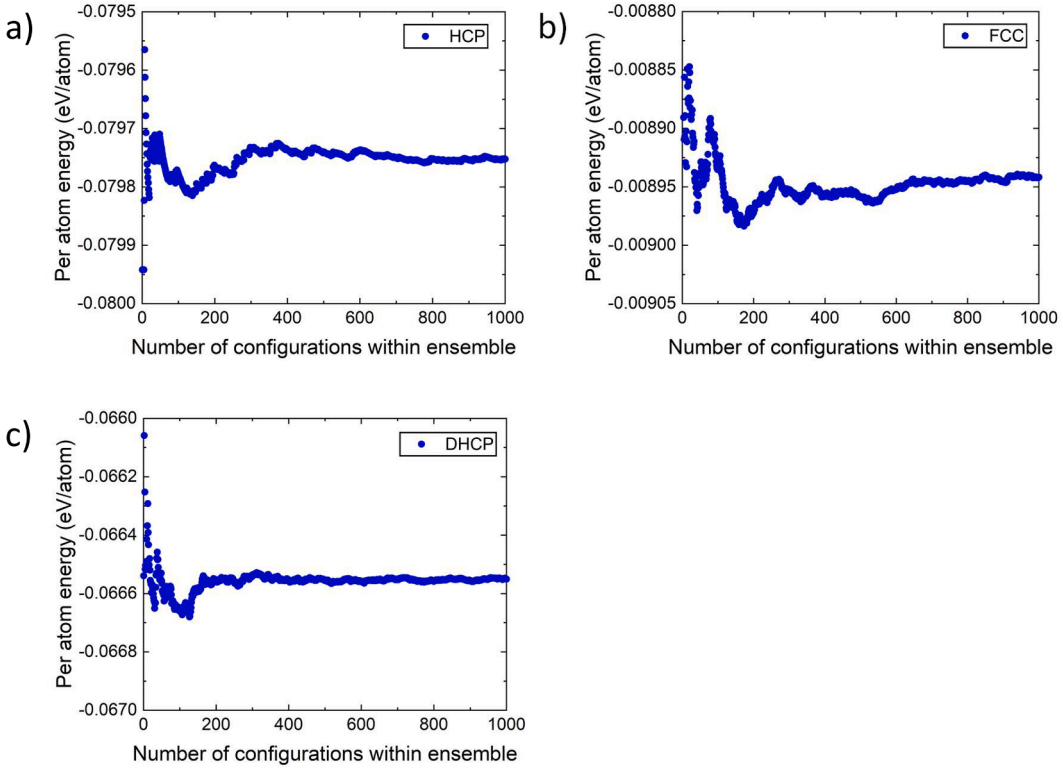

Fig. 3. Typical convergence behavior (using 15 at.% Al in Ni for instance) of the mean per atom energies with respect to the number of configurations generated by MC for three parent lattice types: a) HCP, b) FCC, and c) DHCP.

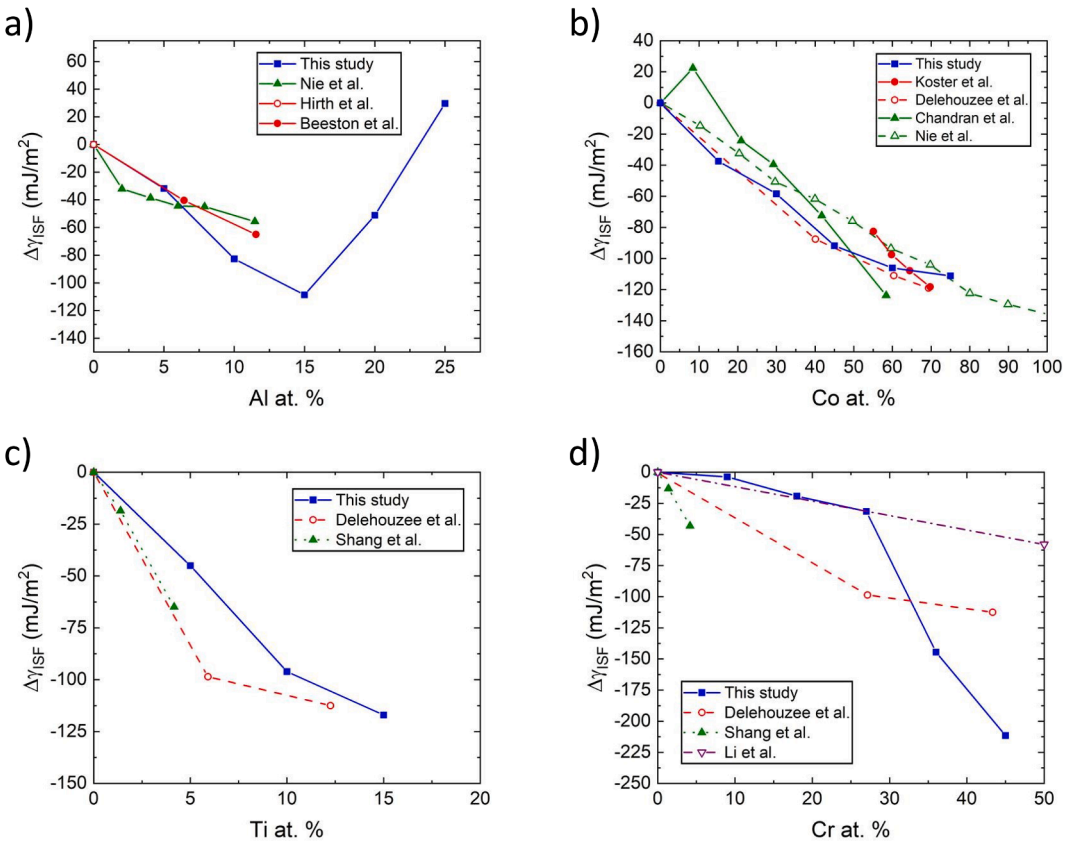

Fig. 4. Variation in SFE ($\Delta\gamma_{ISF}$ with the SFE of pure Ni as reference) as a result of change in solute concentration for a) $Ni_xAl_{(1-x)}$, b) $Ni_xCo_{(1-x)}$, c) $Ni_xTi_{(1-x)}$, and d) $Ni_xCr_{(1-x)}$ alloys.

with the literature. Specially, within 15%, the predicted reducing effect of Ti (~120 mJ/m^2) is more significant than that of Cr in the same concentration range. The literature data on the effect of Ti, although limited, appear to agree fairly well (see Fig. 4(c)) [61,63]. The present work slightly underestimates Ti's reducing effect on SFE. As for Cr, although all literature data consistently suggested that Cr reduces SFE of the Ni based binary alloys, significant scatter exists (Fig. 4(d)) [61,63,64]. The present work's prediction agrees well with the one made by Li et al. [34,64] at Cr at % below 30%. Nevertheless, the overall effect of Cr predicted by this work is in a reasonable agreement with the experimental measurement by Delehouzee et al [61]. The reducing effect of Cr were also highlighted in the theoretical calculation of ternary alloys using first principle calculations [34].

3.4. Synergy of solute content and configurational temperature effects on the SFE of binary alloys

The complete data set obtained from this study showing the combined solute atom concentration and configurational temperature effects on the SFE of the Ni-base binary FCC alloys (measured by the relative SFE, i.e., $\Delta\gamma_{ISF}$) is presented below. The temperature effects captured in this work only arise from the temperature-dependent configurational entropy and do not incorporate the vibrational entropy [65]. As shown in Fig. 5(a), the temperature does not significantly influence the SFE value of Ni-Al alloy. As the concentration of Al increases (up to 15 at.%) the SFE experiences a relative decrease of ~125 mJ/m^2 (see Fig. 5(a)), effectively dropping to 0 on the absolute scale. Further increase in solute concentration increases the SFE. This increasing trend, as discussed in Section 3.3, is somewhat echoed by the experimental data available in the literature that the complex SFE of the Ni_3Al (25% of Al) phase is ~235 mJ/m^2, which is significantly higher than that of the pure Ni or any of the FCC Ni-Al alloys [53,60]. Since Ni_3Al is a thermally stable compound and, as was shown by Dodaran et al. [36] no configurational variations were expected even at elevated temperatures (up to 1100 K), this trend of SFE variation of Ni-Al alloy beyond 15 at.% Al is expected to be valid at different temperatures [53,66].

Variation in the SFE of binary Ni-Co system is presented in Fig. 5(b). At room temperature (300 K), the SFE rapidly decreases with the increasing Co concentration. However, at elevated temperatures, the SFE exhibited a slight increasing then decreasing trend. Overall, the Co concentration does not seem to affect the SFE of the FCC Ni-Co alloy when the configurational entropic effects of higher temperatures (700 K and 1100 K) are considered in the calculations. In the case of the Ni-Co alloy, the temperature appears to strongly influence the SFE. No data, to the best knowledge of the authors, is available in the literature on the SFE of Ni-Co alloys at elevated temperatures. However, the decrease in SFE at room temperature obtained in this study is in perfect agreement with the existing numerical and experimental investigations [29,61,62], as was discussed in Section 3.3.

As shown in Fig. 5(c), the increase in the concentration of Ti significantly decreases the SFE, while the increase in temperature has a similar effect, i.e., increase in temperature from 300 K to 1100 K tends to decrease the SFE as a result of change in configurational entropy. Note that the effect of solute concentration is far more pronounced than that of the configurational temperature effect. Overall, the introduction of 15 at.% Ti solute decreases the SFE by 150 ± 50 mJ/m^2 relative to pure Ni. The Cr concentration and configurational temperature effects on the variation of SFE of the FCC Ni-Cr is shown in Fig. 5(d). As an overall behavior across all temperatures, when Cr is introduced to pure Ni, the change in SFE is not significant up to ~25 at.%. However, the further increase in the concentration of Cr tends to decrease the SFE to a maximum of ~200 mJ/m^2 relative to pure Ni. It is worth noting that the configurational temperature effect is most significant when the Cr

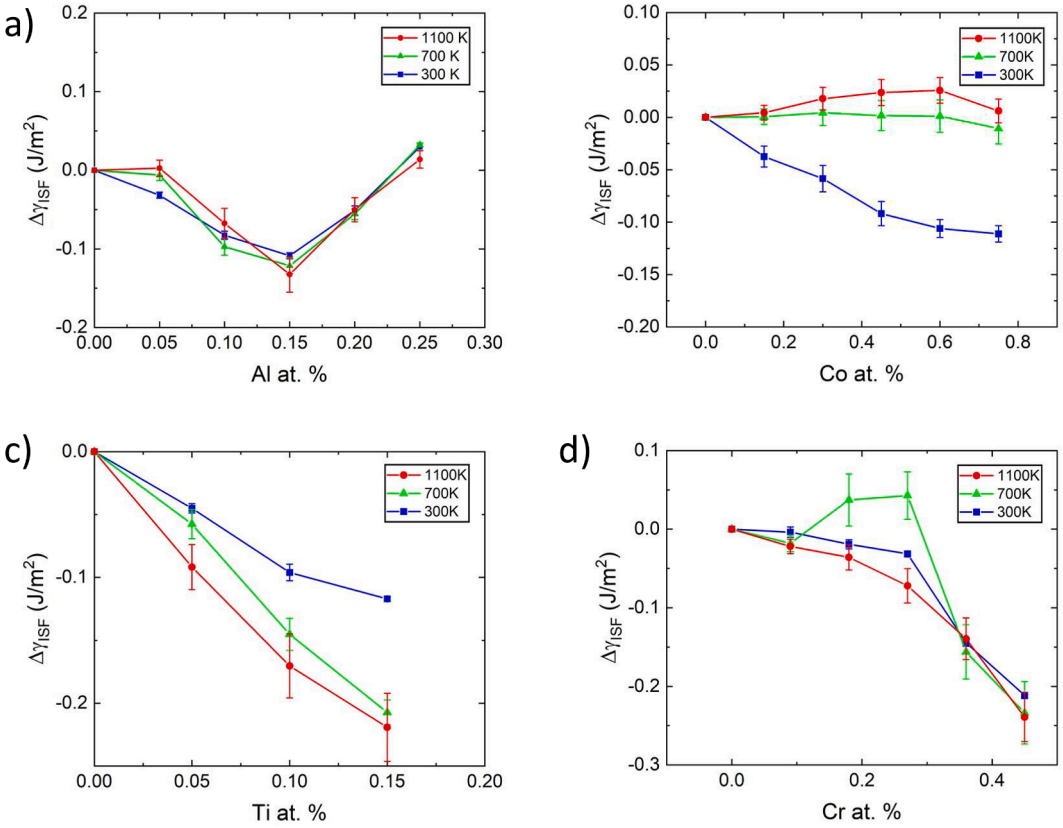

Fig. 5. Synergistic effect of temperature and solute concentration on the SFE ($\Delta\gamma_{ISF}$ with the SFE of pure Ni as reference) of $Ni_xM_{(1-x)}$ alloys with M being a) Al, b) Co, c) Ti, and d) Cr.

concentration is ~25%.

Fluctuations in the SFE (SD(γ_{ISF})) due to the configurational variations in the atomic structures generated by MC, as calculated using Eq. (8), are shown in Fig. 5 as error bars. As shown, in most cases SD(γ_{ISF}) increases with increasing temperature. This is expected since, as mentioned in Section 2.2, the temperature dependent probability assigned for the acceptance of new structures within the MC scheme will increase as the temperature increases, leading to larger configurational variation. Due to the same reason, for thermally stable, ordered compounds such as Ni_3Al, the SD(γ_{ISF}) is expected to be smaller than disordered alloys. Indeed, this is evident in Fig. 5(a) where the fluctuation in the SFE at 25 at.% Al is considerably smaller than other compositions at all temperatures. Similarly, the SD(γ_{ISF}) for pure Ni is always zero since the configurational entropy is zero.

4. Conclusions

In this work, the axial Ising model (AIM) is combined with density functional theory calculations (DFT) and cluster expansion (CE) to investigate the solute concentration and configurational temperature effects on the stacking fault energy (SFE) of binary Ni alloys. The effect of the chemical disorder has been incorporated by evaluating the energies of a minimum of 3000 atomistic structures for each composition using the Monte Carlo (MC) sampling scheme. The CE method is used to calculate the energy of all the structures constructed by MC. The following conclusions can be drawn:

1) Across the entire temperature range of 300 K-1100 K, an increase in Al concentration first decreases and then increases the SFE, while configurational temperature effects on SFE are negligible.
2) An increase in solute concentration in binary FCC $Ni_xTi_{(1-x)}$ alloy significantly decreases the SFE. Configurational variations due to temperature effects further reduces the SFE.
3) An increase in Cr concentration decreases the SFE, while configurational variations due to temperatures does not have a clear and pronounced influence.
4) The addition of Co reduces the SFE of the Ni-Co alloy at room temperature, while not significantly influencing SFE at elevated temperatures.

CRediT authorship contribution statement

Mohammad S. Dodaran: Methodology, Validation, Formal analysis, Investigation, Visualization, Data curation, Writing - original draft. **Shengmin Guo:** Resources, Investigation, Supervision, Writing - review & editing. **Michael M. Khonsari:** Resources, Investigation, Supervision, Writing - review & editing. **Nima Shamsaei:** Resources, Investigation, Supervision, Writing - review & editing. **Shuai Shao:** Conceptualization, Resources, Supervision, Project administration, Funding acquisition, Validation, Investigation, Visualization, Formal analysis, Writing - original draft, Writing - review & editing.

Declaration of Competing Interest

The authors declare that they have no known competing financial interests or personal relationships that could have appeared to influence the work reported in this paper.

Acknowledgement

This material is based upon work supported by the U.S. Department of Energy, Office of Science, Office of Basic Energy Sciences, under

Award Number DE-SC0019378. The authors also thank Prof. Wen Jin Meng for his helpful input. Portions of this research were conducted with high performance computing resources provided by Louisiana State University (http://www.hpc.lsu.edu).

Disclaimer

This report was prepared as an account of work sponsored by an agency of the United States Government. Neither the United States Government nor any agency thereof, nor any of their employees, makes any warranty, express or implied, or assumes any legal liability or responsibility for the accuracy, completeness, or usefulness of any information, apparatus, product, or process disclosed, or represents that its use would not infringe privately owned rights. Reference herein to any specific commercial product, process, or service by trade name, trademark, manufacturer, or otherwise does not necessarily constitute or imply its endorsement, recommendation, or favoring by the United States Government or any agency thereof. The views and opinions of authors expressed herein do not necessarily state or reflect those of the United States Government or any agency FA R&D Special TC NOVEMBER 2017- FF Page 4 of 12 thereof.

Data availability

The raw data required to reproduce these findings are available upon reasonable request. The processed data required to reproduce these findings are available upon reasonable request.

References

[1] D.P. Mourer, E.S. Huron, K.R. Bain, E.E. Montero, P.L. Reynolds, J.J. Schirra, Superalloy optimized for High Temperature Performance in High-pressureturbine Disks (2003) 9.
[2] P. Caron, T. Khan, Evolution of Ni-based superalloys for single crystal gas turbine blade applications, Aerosp. Sci. Technol. 3 (8) (1999) 513–523, https://doi.org/10.1016/S1270-9638(99)00108-X.
[3] N.K. Arakere, G. Swanson, Effect of crystal orientation on fatigue failure of single crystal nickel base turbine blade superalloys, J. Eng. Gas Turbines Power 124 (2002) 161–176, https://doi.org/10.1115/1.1413767.
[4] S.J. Patel, J.J. De Barbadillo, B.A. Baker, R.D. Gollihue, Nickel base superalloys for next generation coal fired AUSC power plants, in: Procedia Eng., Elsevier Ltd, 2013, pp. 246–252, https://doi.org/10.1016/j.proeng.2013.03.250.
[5] H. Zhang, C. Li, Q. Guo, Z. Ma, H. Li, Y. Liu, Improving creep resistance of nickel-based superalloy Inconel 718 by tailoring gamma double prime variants, Scr. Mater. 164 (2019) 66–70, https://doi.org/10.1016/j.scriptamat.2019.01.041.
[6] J.M. Oblak, D.F. Paulonis, D.S. Duvaal, Coherency strengthening in Ni base alloys hardened by D022 γ" precipitates, Metall. Trans. 5 (1974) 143–153.
[7] Y.-Y. Lin, F. Schleifer, M. Fleck, U. Glatzel, On the interaction between γ'' precipitates and dislocation microstructures in Nb containing single crystal nickel-base alloys, Mater. Charact. 165 (2020), https://doi.org/10.1016/j.matchar.2020.110389, 110389.
[8] M.J. Donachie, S.J. Donachie, Superalloys: A Technical Guide, second ed., ASM International, Materials Park, OH, 2002 doi:10.1361.
[9] T.M. Pollock, A.S. Argon, Creep resistance of CMSX-3 nickel base superalloy single crystals, Acta Metall. Mater. 40 (1) (1992) 1–30, https://doi.org/10.1016/0956-7151(92)90195-K.
[10] F. Pettinari, J. Douin, G. Saada, P. Caron, A. Coujou, N. Clément, Stacking fault energy in short-range ordered γ-phases of Ni-based superalloys, Mater. Sci. Eng., A 325 (1-2) (2002) 511–519, https://doi.org/10.1016/S0921-5093(01)01765-8.
[11] M. Benyoucef, B. Décamps, A. Coujou, N. Clément, Stacking-fault energy at room temperature of the γ matrix of the MC2 Ni-based superalloy, Philos. Mag. A 71 (4) (1995) 907–923, https://doi.org/10.1080/01418619508236228.
[12] D.M. Esterling, A.R. McGurn, I.M. Boswarva, R.J. Arsenault, Stacking fault widths, energies and dislocation core structures, Mater. Sci. Eng. 68 (1) (1984) 97–106, https://doi.org/10.1016/0025-5416(84)90247-7.
[13] J.P. Hirth, J. Lothe, Theory of Dislocations, second ed., Krieger Publishing Company, Malabar, FL, 1982.
[14] C.B. Carter, S.M. Holmes, The stacking-fault energy of nickel, Philos. Mag. A J. Theor. Exp Appl. Phys. 35 (1977) 1161–1172, https://doi.org/10.1080/14786437708232942.
[15] D.J.H. Cockayne, V. Vitek, Effect of core structure on the determination of the stacking-fault energy in close-packed metals, Phys. Status Solidi. 65 (2) (1974) 751–764, https://doi.org/10.1002/(ISSN)1521-395110.1002/pssb:v65:210.1002/pssb:2220650236.
[16] Y. Yuan, Y.F. Gu, C.Y. Cui, T. Osada, T. Tetsui, T. Yokokawa, H. Harada, Creep mechanisms of U720Li disc superalloy at intermediate temperature, Mater. Sci. Eng., A 528 (15) (2011) 5106–5111, https://doi.org/10.1016/j.msea.2011.03.034.
[17] W.W. Milligan, S.D. Antolovich, The mechanisms and temperature dependence of superlattice stacking fault formation in the single-crystal superalloy PWA 1480, Metall. Trans. A 22 (10) (1991) 2309–2318, https://doi.org/10.1007/BF02664997.
[18] D.C. Ludwigson, Modified stress-strain relation for FCC metals and alloys, Metall. Trans. 2 (10) (1971) 2825–2828, https://doi.org/10.1007/BF02813258.
[19] T. Rasmussen, K.W. Jacobsen, T. Leffers, O.B. Pedersen, S.G. Srinivasan, H. Jónsson, Atomistic determination of cross-slip pathway and energetics, Phys. Rev. Lett. 79 (19) (1997) 3676–3679, https://doi.org/10.1103/PhysRevLett.79.3676.
[20] T. Rasmussen, K.W. Jacobsen, T. Leffers, O.B. Pedersen, Simulations of the atomic structure, energetics, and cross slip of screw dislocations in copper, Phys. Rev. B. 56 (6) (1997) 2977–2990, https://doi.org/10.1103/PhysRevB.56.2977.
[21] J. Bonneville, B. Escaig, Cross-slipping process and the stress-orientation dependence in pure copper, Acta Metall. 27 (9) (1979) 1477–1486, https://doi.org/10.1016/0001-6160(79)90170-6.
[22] J. Bonneville, B. Escaig, J.L. Martin, A study of cross-slip activation parameters in pure copper, Acta Metall. 36 (8) (1988) 1989–2002, https://doi.org/10.1016/0001-6160(88)90301-X.
[23] A.S. Argon, W.C. Moffatt, Climb of extended edge dislocations, Acta Metall. 29 (2) (1981) 293–299, https://doi.org/10.1016/0001-6160(81)90156-5.
[24] C.K.L. Davies, P.W. Davies, B. Wilshire, The effect of variations in stacking-fault energy on the creep of nickel-cobalt alloys, Phil. Mag. 12 (118) (1965) 827–839, https://doi.org/10.1080/14786436508218920.
[25] C.R. Barrett, O.D. Sherby, Influence of stacking fault energy on high temperature creep of pure metals, Trans. Metall. Soc AIME (1965).
[26] A.K. Mukherjee, J.E. Bird, J.E. Dorn, E. Org, Experimental correlations for high-temperature creep, (1968).
[27] G. Thomas, The effect of short-range order on stacking fault energy and dislocation arrangements in f.c.c. solid solutions, Acta Metall. 11 (12) (1963) 1369–1371, https://doi.org/10.1016/0001-6160(63)90035-X.
[28] S. Crampin, K. Hampel, D.D. Vvedensky, J.M. MacLaren, The calculation of stacking fault energies in close-packed metals, J. Mater. Res. 5 (10) (1990) 2107–2119, https://doi.org/10.1557/JMR.1990.2107.
[29] M. Chandran, S.K. Sondhi, First-principle calculation of stacking fault energies in Ni and Ni-Co alloy, J. Appl. Phys. 109 (10) (2011) 103525, https://doi.org/10.1063/1.3585786.
[30] T.L. Achmad, W. Fu, H. Chen, C. Zhang, Z.-G. Yang, Computational thermodynamic and first-principles calculation of stacking fault energy on ternary co-based alloys, Comput. Mater. Sci. 143 (2018) 112–117, https://doi.org/10.1016/j.commatsci.2017.11.004.
[31] X. Nie, Renhui Wang, Yiying Ye, Yumei Zhou, Dingsheng Wang, Calculations of stacking fault energy for fcc metals and their alloys based on an improved embedded-atom method, Solid State Commun. 96 (10) (1995) 729–734, https://doi.org/10.1016/0038-1098(95)00506-4.
[32] Y. Qi, R.K. Mishra, Ab initio study of the effect of solute atoms on the stacking fault energy in aluminum, Phys. Rev. B. 75 (2007), 224105, https://doi.org/10.1103/PhysRevB.75.224105.
[33] PJH. Denteneer, W.van. Haeringen, Stacking-fault energies in semiconductors from first-principles calculations, J. Phys. C: Solid State Phys. 20 (32) (1987) L883–L887, https://doi.org/10.1088/0022-3719/20/32/001.
[34] L. Vitos, J.-O. Nilsson, B. Johansson, Alloying effects on the stacking fault energy in austenitic stainless steels from first-principles theory, Acta Mater. 54 (2006) 3821–3826, https://doi.org/10.1016/j.actamat.2006.04.013.
[35] R. Sun, C. Woodward, A. van de Walle, First-principles study on N3Al (111) antiphase boundary with Ti and Hf impurities, Phys. Rev. B. 95 (2017), 214121, https://doi.org/10.1103/PhysRevB.95.214121.
[36] M. Dodaran, A.H. Ettefagh, S.M. Guo, M.M. Khonsari, W.J. Meng, N. Shamsaei, S. Shao, Effect of alloying elements on the γ' antiphase boundary energy in Ni-base superalloys, Intermetallics 117 (2020), https://doi.org/10.1016/j.intermet.2019.106670, 106670.
[37] E. Ising, Beitrag zur Theorie des Ferromagnetismus, Zeitschrift Für Phys. 31 (1) (1925) 253–258, https://doi.org/10.1007/BF02980577.
[38] L. Onsager, A two-dimensional model with an order-disorder transition, Phys. Rev. 65 (3-4) (1944) 117–149, https://doi.org/10.1103/PhysRev.65.117.
[39] L. Vitos, PA Korzhavyi, J.-O. Nilsson, B. Johansson, Stacking fault energy and magnetism in austenitic stainless steels, Phys. Scr. 77 (6) (2008) 065703, https://doi.org/10.1088/0031-8949/77/06/065703.
[40] S. Lu, Q.-M. Hu, Börje Johansson, L. Vitos, Stacking fault energies of Mn, Co and Nb alloyed austenitic stainless steels, Acta Mater. 59 (14) (2011) 5728–5734, https://doi.org/10.1016/j.actamat.2011.05.049.
[41] J.M. Sanchez, F. Ducastelle, D. Gratias, Generalized cluster description of multicomponent systems, Phys. A Stat. Mech. Its Appl. 128 (1-2) (1984) 334–350, https://doi.org/10.1016/0378-4371(84)90096-7.
[42] A. van de Walle, M. Asta, G. Ceder, The alloy theoretic automated toolkit: a user guide, Calphad 26 (4) (2002) 539–553, https://doi.org/10.1016/S0364-5916(02)80006-2.
[43] P. Giannozzi, S. Baroni, N. Bonini, M. Calandra, R. Car, C. Cavazzoni, D. Ceresoli, G.L. Chiarotti, M. Cococcioni, I. Dabo, A. Dal Corso, S. de Gironcoli, S. Fabris, G. Fratesi, R. Gebauer, U. Gerstmann, C. Gougoussis, A. Kokalj, M. Lazzeri, L. Martin-Samos, N. Marzari, F. Mauri, R. Mazzarello, S. Paolini, A. Pasquarello, L. Paulatto, C. Sbraccia, S. Scandolo, G. Sclauzero, A.P. Seitsonen, A. Smogunov, P. Umari, R.M. Wentzcovitch, QUANTUM ESPRESSO: a modular and open-source software project for quantum simulations of materials, J. Phys.: Condens. Matter 21 (39) (2009) 395502, https://doi.org/10.1088/0953-8984/21/39/395502.

[44] A. van de Walle, M.D. Asta, A. Walle, G. Ceder, Automating First-principles Phase Diagram Calculations, J. Phase Equilib. 23 (2002) 348–359, https://doi.org/10.1361/105497102770331596.
[45] R. Sun, A. van de Walle, Automating impurity-enhanced antiphase boundary energy calculations from ab initio Monte Carlo, Calphad 53 (2016) 20–24, https://doi.org/10.1016/j.calphad.2016.02.005.
[46] A.van.de. Walle, M. Asta, Self-driven lattice-model Monte Carlo simulations of alloy thermodynamic properties and phase diagrams, Model. Simul. Mater. Sci. Eng. 10 (5) (2002) 521–538, https://doi.org/10.1088/0965-0393/10/5/304.
[47] X. Zhang, B. Grabowski, F. Körmann, A.V. Ruban, Y. Gong, R.C. Reed, T. Hickel, J. Neugebauer, Temperature dependence of the stacking-fault Gibbs energy for Al, Cu, and Ni, Phys. Rev. B. 98 (2018), 224106, https://doi.org/10.1103/PhysRevB.98.224106.
[48] G. Prandini, A. Marrazzo, I.E. Castelli, N. Mounet, N. Marzari, Precision and efficiency in solid-state pseudopotential calculations, npj Comput. Mater. 4 (2018) 72, https://doi.org/10.1038/s41524-018-0127-2.
[49] J.P. Perdew, K. Burke, M. Ernzerhof, Generalized gradient approximation made simple, Phys. Rev. Lett. 77 (18) (1996) 3865–3868, https://doi.org/10.1103/PhysRevLett.77.3865.
[50] F.D. Murnaghan, The compressibility of media under extreme pressures, Proc. Natl. Acad. Sci. 30 (9) (1944) 244–247, https://doi.org/10.1073/pnas.30.9.244.
[51] R.E. Smallman, P.S. Dobson, Stacking fault energy measurement from diffusion, Metall. Trans. 1 (1970) 2383–2389, https://doi.org/10.1007/BF03038367.
[52] H.-L. Chen, E. Doernberg, P. Svoboda, R. Schmid-Fetzer, Thermodynamics of the Al3Ni phase and revision of the Al–Ni system, Thermochim. Acta. 512 (2011) 189–195, https://doi.org/10.1016/j.tca.2010.10.005.
[53] H.P. Karnthaler, E.T. Mühlbacher, C. Rentenberger, The influence of the fault energies on the anomalous mechanical behaviour of Ni3Al alloys, Acta Mater. 44 (2) (1996) 547–560, https://doi.org/10.1016/1359-6454(95)00191-3.
[54] T.B. Massalski, Binary alloy phase diagrams, ASM Int. 3 (1992) 2874.
[55] K. Hagihara, T. Nakano, Y. Umakoshi, Plastic deformation behaviour in Ni3Ti single crystals with D024 structure, Acta Mater. 51 (9) (2003) 2623–2637, https://doi.org/10.1016/S1359-6454(03)00060-0.
[56] P. Nash, The Cr−Ni (Chromium-Nickel) system, Bull. Alloys Phase Diagrams. 7 (5) (1986) 466–476, https://doi.org/10.1007/BF02867812.
[57] G. Venkataraman, Y.-W.W. Chung, Y. Nakasone, T. Mura, Free energy formulation of fatigue crack initiation along persistent slip bands: calculation of S-N curves and crack depths, Acta Metall. Mater. 38 (1990) 31–40, https://doi.org/10.1016/0956-7151(90)90132-Z.
[58] Z. Du, D. Lü, Thermodynamic modeling of the Co–Ni–Y system, Intermetallics 13 (6) (2005) 586–595, https://doi.org/10.1016/j.intermet.2004.09.013.
[59] B.E.P. Beeston, L.K. France, The stacking-fault energies of some binary nickel alloys fundamental to the nimonic series, J. Inst. Met. 96 (1968) 2454.
[60] B.E.P. Beeston, L.K. France, No title, J. Inst. Met. 96 (1968) 2454.
[61] L. Deléhouzée, A. Deruyttere, The stacking fault density in solid solutions based on copper, silver, nickel, aluminium and lead, Acta Metall. 15 (5) (1967) 727–734, https://doi.org/10.1016/0001-6160(67)90353-7.
[62] E.H. Köster, A.R. Thölén, A. Howie, Stacking fault energies of Ni–Co–Cr alloys, Phil. Mag. 10 (108) (1964) 1093–1095, https://doi.org/10.1080/14786436408225417.
[63] S.L. Shang, C.L. Zacherl, H.Z. Fang, Y. Wang, Y. Du, Z.K. Liu, Effects of alloying element and temperature on the stacking fault energies of dilute Ni-base superalloys, J. Phys.: Condens. Matter 24 (50) (2012), https://doi.org/10.1088/0953-8984/24/50/505403, 505403.
[64] C. Li, S. Dang, P. Han, X. He, X. Long, Effect of Cr on the generalized stacking fault energy of impure doped Ni (111) surface: a first-principles study, Eur. Phys. J. B. 93 (2020) 156, https://doi.org/10.1140/epjb/e2020-10013-x.
[65] P.J. Craievich, J.M. Sanchez, Vibrational free energy in the Ni-Cr system, Comput. Mater. Sci. 8 (1-2) (1997) 92–99, https://doi.org/10.1016/S0927-0256(97)00021-9.
[66] Morgan, Summary for policymakers, in: Intergovernmental Panel on Climate Change (Ed.), Clim. Chang. 2013 - Phys. Sci. Basis, Cambridge University Press, Cambridge, 2019, pp. 1–30, https://doi.org/10.1017/CBO9781107415324.004.
[67] I.L. Dillamore, R.E. Smallman, The stacking-fault energy of F.C.C. metals, Phil. Mag. 12 (115) (1965) 191–193, https://doi.org/10.1080/14786436508224959.
[68] R.E. Schramm, R.P. Reed, Stacking fault energies of fcc fe-Ni alloys by x-ray diffraction line profile analysis, Metall. Trans. A 7 (3) (1976) 359–363, https://doi.org/10.1007/BF02642831.
[69] L.E. Murr, Interfacial Phenomena in Metals and Alloys, Addison-Wesley Publishing Company, Reading, MA, 1975.
[70] M.J. Mills, P. Stadelmann, A study of the structure of Lomer and 60° dislocations in aluminium using high-resolution transmission electron microscopy, Philos. Mag. A 60 (3) (1989) 355–384, https://doi.org/10.1080/01418618908213867.
[71] Y. Mishin, Atomistic modeling of the $\gamma{\$}and $\gamma{\$}′-phases of the Ni–Al system, Acta Mater. 52 (2004) 1451–1467, https://doi.org/10.1016/j.actamat.2003.11.026.
[72] B. Hammer, K.W. Jacobsen, V. Milman, M.C. Payne, Stacking fault energies in aluminium, J. Phys.Condens. Matter. 4 (50) (1992) 10453–10460, https://doi.org/10.1088/0953-8984/4/50/033.
[73] R.E. Voskoboinikov, Effective γ-surfaces in 111 plane in FCC Ni and L12 Ni3Al intermetallic compound, Phys. Met. Metallogr. 114 (7) (2013) 545–552, https://doi.org/10.1134/S0031918X13070132.
[74] R.H. Rautioaho, An interatomic pair potential for aluminium calculation of stacking fault energy, Phys. Status Solidi 112 (1) (1982) 83–89, https://doi.org/10.1002/pssb:2221120108.
[75] Y. Mishin, D. Farkas, M.J. Mehl, D.A. Papaconstantopoulos, Interatomic potentials for monoatomic metals from experimental data and ab initio calculations, Phys. Rev. B. 59 (5) (1999) 3393–3407, https://doi.org/10.1103/PhysRevB.59.3393.
[76] C. Woodward, D.R. Trinkle, L.G. Hector, D.L. Olmsted, Prediction of dislocation cores in aluminum from density functional theory, Phys. Rev. Lett. 100 (2008), 045507, https://doi.org/10.1103/PhysRevLett.100.045507.
[77] D.J. Siegel, Generalized stacking fault energies, ductilities, and twinnabilities of Ni and selected Ni alloys, Appl. Phys. Lett. 87 (12) (2005) 121901, https://doi.org/10.1063/1.2051793.
[78] S. Kibey, J.B. Liu, D.D. Johnson, H. Sehitoglu, Predicting twinning stress in fcc metals: linking twin-energy pathways to twin nucleation, Acta Mater. 55 (20) (2007) 6843–6851, https://doi.org/10.1016/j.actamat.2007.08.042.
[79] S. Zhao, G.M. Stocks, Y. Zhang, Stacking fault energies of face-centered cubic concentrated solid solution alloys, Acta Mater. 134 (2017) 334–345, https://doi.org/10.1016/j.actamat.2017.05.001.
[80] G. Lu, N. Kioussis, V.V. Bulatov, E. Kaxiras, Generalized-stacking-fault energy surface and dislocation properties of aluminum, Phys. Rev. B. 62 (5) (2000) 3099–3108, https://doi.org/10.1103/PhysRevB.62.3099.
[81] J.A. Zimmerman, H. Gao, F.F. Abraham, Generalized stacking fault energies for embedded atom FCC metals, Model. Simul. Mater. Sci. Eng. 8 (2) (2000) 103–115, https://doi.org/10.1088/0965-0393/8/2/302.
[82] N. Bernstein, E. Tadmor, Tight-binding calculations of stacking energies and twinnability in fcc metals, Phys. Rev. B. 69 (2004), 094116, https://doi.org/10.1103/PhysRevB.69.094116.
[83] R. Meyer, L.J. Lewis, Stacking-fault energies for Ag, Cu, and Ni from empirical tight-binding potentials, Phys. Rev. B 1–5 (2002).